Journal of Hydro-environment Research 14 (2017) 105–118

Contents lists available at ScienceDirect

Journal of Hydro-environment Research

journal homepage: www.elsevier.com/locate/JHER

Responses of soil moisture to climate change based on projections by the end of the 21st century under the high emission scenario in the 'Huang–Huai–Hai Plain' region of China

Fei Peng [a,c,d], Mu Mu [b,a], Guodong Sun [a,d,*]

[a] State Key Laboratory of Numerical Modeling for Atmospheric Sciences and Geophysical Fluid Dynamics (LASG), Institute of Atmospheric Physics, Chinese Academy of Sciences, Beijing 100029, China
[b] Institute of Atmospheric Sciences, Fudan University, 220 Handan Road, Shanghai 200433, China
[c] Numerical Weather Prediction Center, China Meteorological Administration, Beijing 100081, China
[d] University of Chinese Academy of Sciences, Beijing 100049, China

ARTICLE INFO

Article history:
Received 30 June 2015
Revised 28 September 2016
Accepted 11 October 2016
Available online 15 November 2016

Keywords:
Soil moisture
Extreme climate
CNOP-P
CoLM

ABSTRACT

Based on the future potential projections in the late 21st century under the Representative Concentration Pathway (RCP) 8.5 scenario, the maximal responses of surface soil moisture (SSM) to an extreme climate change are exhibited in the 'Huang–Huai–Hai Plain' ('3H') region of China. The Common Land Model (CoLM) and the approach of conditional nonlinear optimal perturbation related to parameters (CNOP-P) are employed to explore the above issue. Three climate change scenarios, associated with temperature change, precipitation change and changes in both temperature and precipitation, are provided by applying the CNOP-P approach and denoted as the CNOP-P-type temperature change scenario, the CNOP-P-type precipitation change scenario and the CNOP-P-type climate change scenario, respectively. For the CNOP-P-type scenarios, the changes in both climatology and climate variability relative to the reference climate condition are included. To explore the different responses of SSM to different types of climate scenarios, the hypothesized climate change scenarios are examined as well, in which only the change in climatology is considered. Numerical results have suggested that the CNOP-P-type scenario induces greater SSM responses in terms of variation magnitudes than the hypothesized climate change does, especially in the semi-arid regions north of 35°N. For the two types of climate change scenarios, the differences about precipitation and soil ice changes result in the difference about SSM changes in the northern region, though the difference about evapotranspiration variations helps to narrow the difference about SSM. The above results imply that climate variability is important to SSM in the semi-arid region.

1. Introduction

As a key component of climate system, soil moisture has been addressed to improve the sub-seasonal and seasonal forecasting for precipitation (Kanae et al., 2006; Koster et al., 2010), and impose vital impacts on climate extremes (Liu et al., 2014). In addition, as the water stored in unsaturated soil zone, soil moisture is the main natural water resources for agriculture and natural vegetation, and directly associated with agricultural drought (Heim, 2002). Thus, real-time soil moisture measurements play an important role in both crop monitoring and drought warning. Accordingly, changes in soil moisture are vital for assessing the impacts of climate change on agricultural production and natural ecosystems (Kim and Wang, 2012; Tao et al., 2003).

Climate change is one of the primary factors (also including soil texture, topography, vegetation, and so on) that influence soil moisture (Mostovoy and Anantharaj, 2008; Seneviratne et al., 2010; Wilson et al., 2004). Many studies have investigated the responses of soil moisture to recent or future climate change (Seager et al., 2013; Yang et al., 2011). Due to the scarcity of in situ measurements, soil moisture simulated by global circulation models (GCMs) or land surface models (LSMs) has always been employed in the climate change researches. In the study of Seager et al. (2013), model ensembles based on 16 GCMs from Phase 5 of the Coupled Model Intercomparison Project (CMIP5) under the

* Corresponding author at: State Key Laboratory of Numerical Modeling for Atmospheric Sciences and Geophysical Fluid Dynamics (LASG), Institute of Atmospheric Physics, Chinese Academy of Sciences, Beijing 100029, China (G. Sun).
E-mail address: sungd@mail.iap.ac.cn (G. Sun).

http://dx.doi.org/10.1016/j.jher.2016.10.003
1570-6443/

Representative Concentration Pathway (RCP) 8.5 scenario revealed that the annual mean soil moisture would be reduced in the near future (2021–2040) in California and Nevada, the Colorado River headwaters and Texas but less than 5%. Over Tibetan Plateau, Yang et al. (2011) found that the annual mean surface soil moisture was simulated to increase at many locations in the transitional zones (the central Tibetan Plateau) due to recent climate change (1984–2006) by using a simple biosphere scheme (SiB2), but the magnitudes of the trends were quite weak (about 0.001 $m^3 m^{-3}$ per decade).

Although the projections of future climate change may be uncertain, China would probably experience dramatic changes in extreme weather and climate events in the end of the 21st century (Chen et al., 2012; Chen, 2013; Jiang et al., 2012). For heavy rainfall in South China, its frequencies at the end of the 21st century are predicted to increase by 35.9–50.2% and intensities are expected to increase by 2.8–6.3%, relative to the period 1980–1999 (Chen et al., 2012). According to the PRECIS (Providing REgional Climates for Impacts Studies) climate model and the IPCC (Intergovernmental Panel on Climate Change) SRES (Special Report on Emissions Scenarios) B2 scenario, Zhang et al. (2006) reported a higher (lower) occurrence of hot (cold) events over China in the period 2071–2100. And the incidences of severe and extreme drought are predicted to dramatically increase in the future, based on the multi-model projections of CMIP5 GCMs (Wang and Chen, 2014). Besides, the amounts of flooding will increase in the late 21st century (Chen et al., 2012). In response to these possible extreme future climate changes, how about the changes in soil moisture are? The answer to this question may provide a basis to develop climate adaptation strategies in agriculture and water resources. Up to now, the researches focused on the hydrological responses to extreme climate change are scarce, especially in China. Dan et al. (2012) had used the variable infiltration capacity (VIC) model to project the changes in hydrological variables under the hypothesized climate change scenarios. They reported that the changes of soil moisture in the top 10 cm soil layer averaged over the Huang-Huai-Hai Plain (3H) region of China fluctuated from −0.001 to +0.007 $m^3 m^{-3}$ with a 5 °C warming or a +30% precipitation change, which could bound the future climate change in the 3H region due to global warming. But in the hypothesized climate scenarios, the change in climate variability is not taken into account.

To explore the impacts of the changes in both climatology and climate variability on soil moisture under extreme climate change, a new type of climate change scenario is provided in this study by using the Conditional Nonlinear Optimal Perturbation related to model parameters (CNOP-P) approach (Mu et al., 2010). Besides, the maximal responses of soil moisture to an extreme condition of future potential climate change in a region (30° to 40°N, 110° to 120°E) located in East China are discussed by employing the Common Land Model (CoLM, Dai et al., 2003). This study region includes one of the nine principal agricultural zones in China, in which soil moisture plays an important role in agricultural activities and could affect local climate conditions (Zuo and Zhang, 2007; Zhang and Zuo, 2011). The future extreme climate change considered in our study is hypothesized to fluctuate within certain ranges, which are determined according to the uncertainty in projected climate change from 22 GCMs by the end of the 21st century under the high emission scenario RCP8.5. Moreover, the impacts of climate change on surface soil moisture (i.e. soil moisture in the top 10 cm soil; SSM for short) are mainly focused on. The CNOP-P approach could permit us to simultaneously consider the changes in both climatology and climate variability, and has been applied in analyses of the responses of terrestrial ecosystem carbon cycle, such as soil carbon and net primary production, to climate change (Sun and Mu, 2012, 2013, 2014).

2. Study region, model, method and experimental design

2.1. Study region

The study region, located in East China, covers the area from 30° to 40°N and from 110° to 120°E. It contains the Huang-Huai-Hai Plain (3H) region extending from 113°E to the coastline and from 32° to 40.5°N, one of the nine principal agricultural zones in China, where soil moisture variation is vital for crop yields (Dan et al., 2012). Moreover, the precipitation could be influenced through cooling land surface and reduce the land-sea temperature gradient (Zuo and Zhang, 2007; Zhang and Zuo, 2011). The study region is bigger than the real 3H region and thus referred to as the '3H' region for convenience. Based on the study of Ma and Fu (2005), the north of 35°N of the '3H' region is semi-arid region, while the south of 35°N of the '3H' region is humid and semi-humid regions.

2.2. Model

2.2.1. Introduction of the CoLM model

The CoLM model, developed by Dai et al. (2003), comprehensively includes the biophysical, biochemical, ecological and hydrological processes and their interaction. Extensive offline simulations have demonstrated that CoLM has the ability to simulate different land surface processes reasonably (Liu and Lin, 2005; Song et al., 2009; Xin et al., 2006). In terms of hydrological processes, there are 10 soil layers to compute the soil moisture. Among 10 soil layers, in the top five layers, the ice, snow and snow melt are calculated. And, the freezing and thawing cycle processes are also embodied in the CoLM model. The vertical soil moisture transport is governed by infiltration, runoff, gradient diffusion, gravity, and soil water extraction through roots for canopy transpiration. Hence, the CoLM model could realistically seize the alternating wet and dry periods in the top soil (Dai et al., 2003). The experimental results also showed that the bias and root-mean-square error (RMSE) of the snow depth simulations could be reduced using data assimilation schemes in the Altay region of China (Xu and Shu, 2014). The CoLM model was also coupled to Beijing Normal University Earth System Model (BNU-ESM), which could simulate the climatological annual cycle of surface-air temperature and precipitation (Ji et al., 2014).

In the CoLM model, the total soil column with a depth of 3.43 m is divided into 10 unevenly spaced layers. Soil water content within each layer is computed based on the water balance equation. Soil ice is also computed separately. In each soil layer, soil moisture is firstly updated by the melting of soil ice or freezing of soil water, and then altered based on the net water input from the adjacent soil layers and the transpiration if roots exist. The depth of the first three soil layers in CoLM is 9.06 cm. Thus, surface soil moisture (i.e. the soil moisture of the top 10 cm soil layer; SSM for short) is calculated as the weighted average of the soil moisture in the first three soil layers based on soil layer thicknesses. For the surface soil layer, the net water input is mainly associated with precipitation, evapotranspiration (ET) and surface runoff (Rsur).

2.2.2. Forcing dataset

The forcing dataset used in this study comes from the Princeton University (Sheffield et al., 2006), which is a high-resolution (1.0° × 1.0°, 3-hourly), global, meteorological forcing dataset for driving LSMs. It has been used to study soil moisture in China (Li and Ma, 2010; Wang et al., 2011). And the dataset located in our study region from 1991 to 2000 has been interpolated to a 30-min temporal resolution to drive CoLM for conducting simulations as the reference climate conditions.

2.3. The conditional nonlinear optimal perturbation related to parameter (CNOP-P)

The CNOP approach (Mu et al., 2003) was firstly developed to search the optimal initial perturbations without considering model errors. It has been employed in researches of ENSO predictability (Duan and Mu, 2006; Duan et al., 2004), the thermohaline circulation (Mu et al., 2004), adaptive observations of typhoons (Mu et al., 2009; Qin et al., 2013), grassland ecosystems (Mu and Wang, 2007), ensemble prediction (Mu and Jiang, 2008) and the predictability of the Kuroshio Large Meander (Wang et al., 2012, 2013). Through comprehensively taking the sources of predictability errors into account, it was extended to identify the optimal mode of the initial and model parameter perturbations (CNOP-I and CNOP-P) (Mu et al., 2010). And the CNOP approach just for initial perturbations and only for parameter perturbations are referred to as the CNOP-I approach and the CNOP-P approach, respectively. Until now, the CNOP-P approach has been applied to study the ENSO predictability (Duan and Zhang, 2010; Yu et al., 2011), explore the impacts of human activities and climate change on a grassland ecosystem (Sun and Mu, 2011), evaluate the responses of terrestrial ecosystem to changing climate (Sun and Mu, 2012, 2013, 2014) and calibrate model parameters (Wang and Huo, 2013).

In this paper, only the introduction to the CNOP-P approach is presented. For interested readers, details about the CNOP approach could be referred to Mu et al. (2010). Assume the nonlinear differential equations as follows:

$$\begin{cases} \frac{\partial \boldsymbol{U}}{\partial t} = F(\boldsymbol{U}, \boldsymbol{P}) \quad \boldsymbol{U} \in R^n, t \in [0, T] \\ \boldsymbol{U}|_{t=0} = \boldsymbol{U}_0 \end{cases}, \tag{1}$$

where F is a nonlinear operator; $\boldsymbol{U}_0$ represents an initial value of the state variable $\boldsymbol{U}$; and $\boldsymbol{P}$ stands for a parameter vector. Assume that M_t is the propagator of Eq. (1). Then, the solution $\boldsymbol{U}(t)$ equals $M_t(\boldsymbol{U}_0, \boldsymbol{P})$. A perturbation to the parameter vector $\boldsymbol{P}$, denoted as $\boldsymbol{p}$, is supposed. And the solution of Eq. (1) turns into $M_t(\boldsymbol{U}_0, \boldsymbol{P}+\boldsymbol{p})$ and is denoted by $\boldsymbol{U}(t)+\boldsymbol{u}(t)$. Here, $\boldsymbol{u}(t)$ describes the change of the reference state $\boldsymbol{U}(t)$ caused by the parameter perturbation $\boldsymbol{p}$.

For a given time T and norm, the parameter perturbation $\boldsymbol{p}_\delta$ is called a CNOP-P with the constraint condition $\boldsymbol{p} \in \Omega$ if and only if,

$$J(\boldsymbol{p}_\delta) = \max_{\boldsymbol{p}\in\Omega} J(\boldsymbol{p}), \tag{2}$$

where

$$J(\boldsymbol{p}) = \|\boldsymbol{u}(T)\| = \|M_T(\boldsymbol{U}_0, \boldsymbol{P}+\boldsymbol{p}) - M_T(\boldsymbol{U}_0, \boldsymbol{P})\|. \tag{3}$$

Here, $\boldsymbol{P}$ is a reference state of parameters and generally represents the standard parameter values of a model. $\boldsymbol{p}$ is the parameter perturbation to the reference state and stands for the parameter errors. The CNOP-P stands for a kind of parameter perturbation, which satisfies certain constraints and brings about the maximal departure from the reference state at the prediction time T. In this paper, $\boldsymbol{P}$ is taken as the forcing parameters associated with temperature or precipitation and $\boldsymbol{p}$ could be regarded as the changes in temperature or precipitation. In this study, the CNOP-P is regarded as the kind of climate change which could lead to the variations in both climatology and climate variability, and causes the maximal variations of soil moisture.

2.4. Experimental design

To comprehensively evaluate the impacts of extreme climate change on SSM in the case of considering the changes in both climatology and climate variability, a new climate change scenario will be proposed using the CNOP-P approach. It differs from the hypothesized climate change scenarios (Mehrotra, 1999; Singh and Bengtsson, 2004), in which perturbations to the reference temperature series or percentage variations of the reference precipitation series are supposed to be constant. In this study, the soil moisture is corresponding to the state variable U of Eq (1), and the temperature and precipitation is corresponding to the parameters P of Eq (1)

In the new climate change scenario, perturbations to the annual temperature and precipitation, which are time-dependent variables, are taken into account. For temperature, the time-dependent perturbations $p_{t,i}$ satisfy the following conditions:

$$\frac{\sum_{i=1}^{k}\sum_{j=1}^{12}\sum_{m=1}^{d(i,j)}\sum_{n=1}^{r}(P_{t,i,j,m,n}+p_{t,i})}{r\times\sum_{i=1}^{k}\sum_{j=1}^{12}d(i,j)} = \frac{\sum_{i=1}^{k}\sum_{j=1}^{12}\sum_{m=1}^{d(i,j)}\sum_{n=1}^{r}P_{t,i,j,m,n}}{r\times\sum_{i=1}^{k}\sum_{j=1}^{12}d(i,j)} + \delta_t \tag{4}$$

$$0 \leqslant p_{t,i} \leqslant \sigma_t. \tag{5}$$

Here, subscripts i, j and m represent the year, month and day in turn; $d(i,j)$ is the number of days in a month; r represents the number of measurements conducted in a day, which depends on the temporal resolution of the forcing dataset. For example, $r = 48$ corresponds to a temporal resolution of 30 min. And n stands for the time when a measurement is taken on a particular day. P_t stands for the reference state of the forcing parameters with respect to temperature (i.e. the reference temperature series). δ_t is a constant, representing the variation of temperature climatology induced by the time-variant temperature changes. Generally, it is determined by the climate change projections in the region of interest. Moreover, the perturbations superposed on the annual temperature (i.e. $p_{t,i}$) are bounded. The upper bound is σ_t, describing the maximum increase in the annual temperature.

And the perturbations to the annual total precipitation for each year ($p_{p,i}$) are satisfied by the equations as follows:

$$\frac{\sum_{i=1}^{k}p_{p,i}}{k} = \frac{\sum_{i=1}^{k}\sum_{j=1}^{12}\sum_{m=1}^{d(i,j)}\sum_{n=1}^{r}P_{p,i,j,m,n}}{k}\times\frac{p}{100} \tag{6}$$

$$0 \leqslant p_{p,i} \leqslant \sigma_p \tag{7}$$

Here, P_p denotes the reference state of the forcing parameters associated with precipitation (i.e. the reference precipitation series). Similar to δ_t, p is a constant as well, but representing the percentage change of precipitation climatology induced by the time-variant precipitation variations. And it is also determined by the climate change projections in the region of interest. Besides, the perturbations superposed on the annual total precipitation (i.e. $p_{p,i}$) are bounded. The upper bound is σ_p, describing the maximum increase of the annual total precipitation. Then, the percentage change $Q_{p,i}$ for precipitation in each year could be obtained by the formulation:

$$Q_{p,i} = \frac{p_{p,i}}{\sum_{j=1}^{12}\sum_{m=1}^{d(i,j)}\sum_{n=1}^{r}P_{p,i,j,m,n}}\times 100. \tag{8}$$

In brief, precipitation in each time step of the CoLM model ($P_{p,i,j,m,n}$) increases by $Q_{p,i}$ and the total precipitation satisfies the following equation:

$$\frac{\sum_{i=1}^{k}\sum_{j=1}^{12}\sum_{m=1}^{d(i,j)}\sum_{n=1}^{r}\left(P_{p,i,j,m,n}\times\left(1+\frac{Q_{p,i}}{100}\right)\right)}{k} = \frac{\sum_{i=1}^{k}\sum_{j=1}^{12}\sum_{m=1}^{d(i,j)}\sum_{n=1}^{r}P_{p,i,j,m,n}}{k}\times\left(1+\frac{p}{100}\right). \tag{9}$$

To sum up, Eqs. (4) and (5) exhibit how the time-variant temperature perturbations are added to the reference temperature series. So are the Eqs. (6)-(9), but for precipitation. Moreover, the temperature or precipitation changes fluctuate in a certain range,

which is dependent on the uncertainty of the projected temperature or precipitation change. Due to different perturbations between years, the new kind of climate change scenario not only leads to the change in temperature or precipitation climatology, but also results in the variation in the temperature or precipitation variability denoted by the standard deviation.

There are many scenarios satisfying the constraints Eqs. (4)-(9). By employing the CNOP-P method, a kind of temperature or precipitation change scenario, which could not only lead to the variations of climate variability but also induce the maximal responses of SSM within certain reasonable range of climate change, could be identified from all possible scenarios characterized by Eqs. (4)-(9). For convenience, this kind of scenario is denoted as the CNOP-P-type temperature or precipitation change scenario.

Our study period is from 1991 to 2000, during which the temperature and precipitation series are deemed as the reference climate condition, and thus k equals 10. In order to determine the parameters for calculating the CNOP-Ps (i.e. δ_t, σ_t, p, and σ_p), future climate change needs to be projected. Based on 22 GCMs (listed in Table 1) and a higher emission scenario RCP8.5 from CMIP5 (Taylor et al., 2012), the temperature and precipitation changes averaged over the '3H' region for three time slices (2071–2080, 2081–2090 and 2091–2100) relative to the study period 1991–2000 are calculated, shown in Table 2. In terms of multi-model ensemble, temperature would increase by about 5 °C and precipitation would increase but by less than 20% in the late 21st century. Among these GCMs, great uncertainties exist in the projected precipitation changes. From the result of a single model, the maximal increase could attain about 45%; meanwhile the decrease in precipitation (10% or so) is also expected. Finally, a 5 °C increase in the mean state of temperature (i.e. $\delta_t = 5$) and a 30% increase in the mean state of precipitation (i.e. p = 30) are hypothesized. And the maximal annual temperature perturbation is 7.5 °C (i.e. $\sigma_t = 7.5$). For precipitation, the maximal perturbation equals 30% of the maximal annual total precipitation (i.e. $\sigma_p = \max_{i=1,k}\left(\sum_{j=1}^{12}\sum_{m=1}^{d(i,j)}\sum_{n=1}^{r}P_{p,i,j,m,n}\right) \times 30\%$).

It should be noted that SSM is chosen as a variable in the cost function [Eq. (3)]. And the value of the cost function stands for the variation magnitude of SSM in the last year of the study period due to climate change. However, it is possible that the cost function [Eq. (3)] about parameters is non-differentiable, which makes the derivative-based optimization approaches unavailable in calculating the CNOP-Ps. Evolutionary algorithms, by which the optimization problems could be settled without gradient information, may be powerful tools to obtain the CNOP-Ps. So far, such algorithms have been used to conduct parameter estimates and analyze the uncertainty of LSMs (Duan et al., 1992; Yapo et al., 1998). In this paper, the Differential Evolution (DE) algorithm (Storn and Price, 1997), an evolutionary algorithm, was employed to acquire the CNOP-Ps (namely the CNOP-P-type climate change scenario). Recently, it has been adopted to calculate CNOP-Ps for investigating the responses of soil carbon and net primary production to climate change (Sun and Mu, 2012, 2013, 2014). There are 121 grid points from 30° to 40°N and from 110° to 120°E be chosen concurrently to calculate the variation of soil moisture. To obtain the CNOP-P-type climate change scenario in each grid points, 20 random samplings in the DE algorithm are chosen to optimize Eq. (2).

Table 1
List of 22 GCMs from CMIP5 used in our study and their spatial resolution. Besides, only soil moisture simulations from the GCMs in bold font are employed in the following.

Model	Country of origin	Horizontal resolution (Lat × Lon)
ACCESS1-0	Australia	1.875° × 1.25°
bcc-csm1-1	China	~2.8° × 2.8°
BNU-ESM	China	~2.8° × 2.8°
CanESM2	Canada	~2.8°× 2.8°
CCSM4	USA	1.25°× 0.9°
CNRM-CM5	France	~1.4° × 1.4°
CSIRO-Mk3-6-0	Australia	1.875° × 1.875°
Fgoals-g2	China	2.8125° × 3°
Fgoals-s2	China	~2.81° × 1.66°
GFDL-CM3	USA	2.5° × 2°
GISS-E2-R	USA	2.5° × 2°
HadGEM2-AO	Korea	1.875° × 1.25°
HadGEM2-CC	United Kingdom	1.875° × 1.25°
HadGEM2-ES	The sane as above	1.875° × 1.25°
inmcm4	Russia	2° × 1.5°
IPSL-CM5A-LR	France	3.75° × 1.875°
IPSL-CM5A-MR	France	2.5° × 1.25°
MIROC5	Japan	~1.4° × 1.4°
MIROC-ESM	Japan	~2.8° × 2.8°
MPI-ESM-LR	Germany	1.875° × 1.875°
MRI-CGCM3	Japan	1.125°° × 1.125°
NorESM1-M	Norway	2.5° × 1.875°

Table 2
Projections of changes in temperature and precipitation averaged over the '3H' region from the reference period (1991–2000) to the projection period (2071–2080, 2081–2090 and 2091–2100) based on 22 GCMs under the RCP8.5 emission scenario from CMIP5. The values in the parentheses are the minimum and maximum changes from the models, respectively.

Time slices	Temperature (°C)	Precipitation (%)
2071–2080	4.3 (2.6–5.8)	15.1(−14.8–40.1)
2081–2090	4.9 (3.3–6.7)	16.6(−11.8–33.5)
2091–2100	5.6 (3.5–7.0)	19.8 (−6.6–47.8)

Similarly, the hypothesized climate change scenarios could be illustrated by the Eqs. (10) and (11) as follows:

$$\frac{\sum_{i=1}^{k}\sum_{j=1}^{12}\sum_{m=1}^{d(i,j)}\sum_{n=1}^{r}(P_{t,i,j,m,n}+\delta_t)}{r\times\sum_{i=1}^{k}\sum_{j=1}^{12}d(i,j)} = \frac{\sum_{i=1}^{k}\sum_{j=1}^{12}\sum_{m=1}^{d(i,j)}\sum_{n=1}^{r}P_{t,i,j,m,n}}{r\times\sum_{i=1}^{k}\sum_{j=1}^{12}d(i,j)}+\delta_t \tag{10}$$

$$\frac{\sum_{i=1}^{k}\sum_{j=1}^{12}\sum_{m=1}^{d(i,j)}\sum_{n=1}^{r}P_{p,i,j,m,n}\times\left(1+\frac{p}{100}\right)}{r\times\sum_{i=1}^{k}\sum_{j=1}^{12}d(i,j)} = \frac{\sum_{i=1}^{k}\sum_{j=1}^{12}\sum_{m=1}^{d(i,j)}\sum_{n=1}^{r}P_{p,i,j,m,n}}{r\times\sum_{i=1}^{k}\sum_{j=1}^{12}d(i,j)}\times\left(1+\frac{p}{100}\right). \tag{11}$$

In this kind of scenarios, perturbations to the reference temperature series (δ_t) or percentage variations in the reference precipitation series (p) are constant. As a result, the hypothesized scenarios only cause the changes in climatology, and don't induce the variations in climate variability.

Based on above analyses, we can see that there are some similarities and differences between the CNOP-P-type scenarios and the hypothetical ones. The two scenarios supply the reasonable climate change scenarios under the same constraints based on the results of 22 GCMs (Eqs. (4) and (5)). And, the increasing extents of temperature and precipitation are same for two climate change scenarios. However, there are essential differences about the two climate change scenarios. Although the increasing extents of temperature and precipitation are same for two climate change scenarios, the type of variations of temperature and precipitation is different. The CNOP-P-type climate change scenario supplies a statistical forcing and permits that the variability of temperature and precipitation changes according the uncertainty range and statistics results of 22 GCMs. The linear type climate change scenario assumes constant percentage temperature and precipitation rise scenario. Furthermore, the maximal uncertainty of estimated soil

moisture could be obtained under the CNOP-P-type climate change scenario. The variation of soil moisture due to the linear type climate changes is located in the range of variation of soil moisture due to the CNOP-P-type climate change scenario.

3. Results and analysis

3.1. Responses of SSM to extreme climate change related to temperature and precipitation

From the definition of CNOP-P, the changes in SSM under the CNOP-P-type scenarios reflect the maximal responses of SSM to climate change within certain assumptions (i.e. the projected change ranges associated with temperature and precipitation from 22 CMIP5 GCMs) characterized by Eqs. (7) and (9). Figs. 1 and 2 shows the CNOP-P-type climate change scenarios as the driving data to run the CoLM model based on outputs of the 22 GCM models. In the following, the maximal responses of SSM to extreme climate change conditions associated with only temperature, only precipitation, and the combination of temperature and precipitation will be exhibited successively. For convenience, the CNOP-P-type scenarios associated with only temperature, only precipitation, and both temperature and precipitation are denoted as the CNOP-P-type temperature change scenario, the CNOP-P-type precipitation change scenario, and the CNOP-P-type climate change scenario, successively. The introductions to the three CNOP-P-type scenarios are provided in Table 3. Furthermore, the reasons for the changes in SSM due to each CNOP-P-type scenario are also analyzed by investigating variations in the components of surface water budget (i.e. precipitation, surface soil ice, ET, and Rsur) and surface soil temperature (Tss).

3.1.1. Responses of SSM to extreme climate change only related to temperature

In this section, the maximal possible responses of SSM to an extreme condition just associated with temperature are discussed. Relative to the reference state in 2000, the change of SSM induced by the CNOP-P-type temperature change scenario (Figs. 1a and 2a) varied with regions (Fig. 3a1). In the north of 36°N of the study region, SSM increased; while in the south, it decreased. Generally, the SSM change varied in the range from −0.019 to +0.023 $m^3 m^{-3}$ (−7.1% to +18.8%).

In the CNOP-P-type temperature scenario, temperature is hypothesized to rise while precipitation is kept unaltered. Over the north of 36°N, ET and Rsur were almost unchanged although higher air temperature appeared (Fig. 3c1 and d1). The strong soil ice melting implied by the decrease of surface soil ice (Fig. 3b1) was caused by the strongly increased Tss due to climate warming (Fig. 3e1), and mainly contributed to the SSM increase. In the south, soil ice and Rsur changed slightly (Fig. 3b1 and d1). And the increase in Tss was smaller than that in the north (Fig. 3e1). It is the significantly enhanced ET (Fig. 3c1) that led to the decrease of SSM.

3.1.2. Responses of SSM to extreme climate change only related to precipitation

The maximal possible impacts of a kind of extreme precipitation change on SSM are also investigated. Due to the CNOP-P-type precipitation change scenario (Figs. 1b and 2b), SSM increased in the '3H' region (Fig. 4a1). And this increase was more remarkable in the north of 35°N. On the whole, the SSM change varied in the range from +0.008 to +0.034 $m^3 m^{-3}$ (2.5–19.8%).

Soil moisture mainly comes from precipitation. It is not surprising that the CNOP-P-type precipitation change scenario, in which precipitation is hypothesized to increase and temperature is kept unchanged, made SSM increase in the whole study region. The north of 35°N is located in the semi-arid zone. For the drier soil in this region, increased precipitation could easily enter into the surface soil layer and made Rsur change small (Fig. 4d1). ET was primarily limited by precipitation (Seneviratne et al., 2010) and thus strongly enhanced due to more precipitation (Fig. 4c1). Tss decreased slightly (Fig. 4e1), leading to the small increase of soil ice (Fig. 4b1). It is the increased precipitation that mainly contributed to the increase of SSM, although increased soil ice and enhanced ET prevented this increase (Fig. 4b1 and c1). And in the south, semi-humid and humid zones are distributed, where precipitation is easily converted into Rsur. Because precipitation increased, Rsur was strongly augmented (Fig. 4d1). However, both Tss and soil ice were almost unaltered (Fig. 4b1 and c1). ET in this

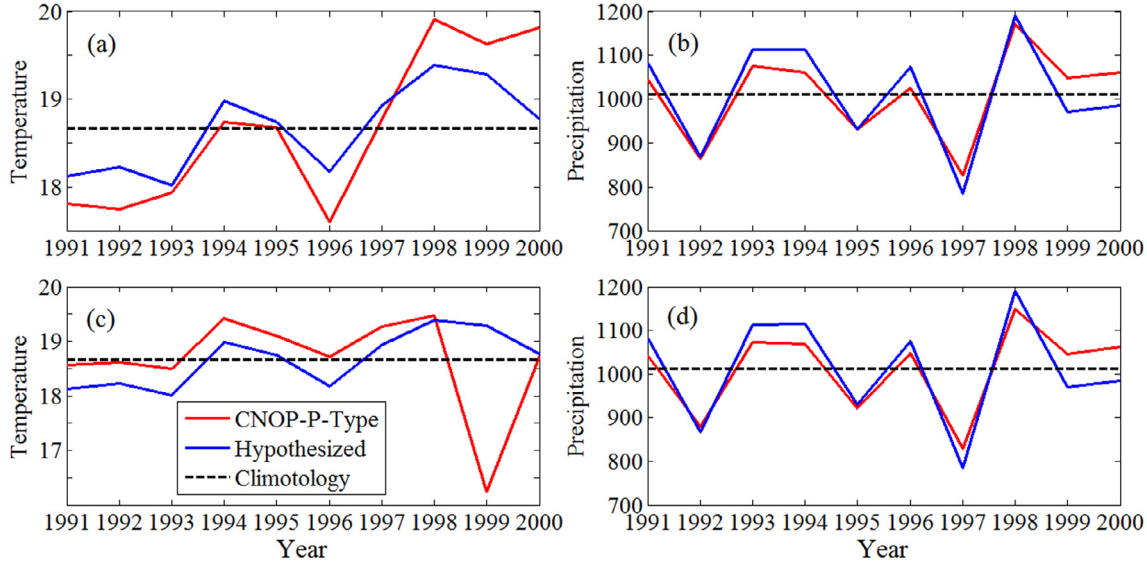

Fig. 1. Annual mean temperature (°C) and precipitation (mm/year) averaged over the '3H' region from 1991 to 2000: (a) temperature under the CNOP-P-type and hypothesized temperature change scenarios; (b) precipitation under the CNOP-P-type and hypothesized precipitation change scenarios; (c) temperature and (d) precipitation under the CNOP-P-type and hypothesized climate change scenarios (including changes in both temperature and precipitation). For the legend, it applies to all of the charts.

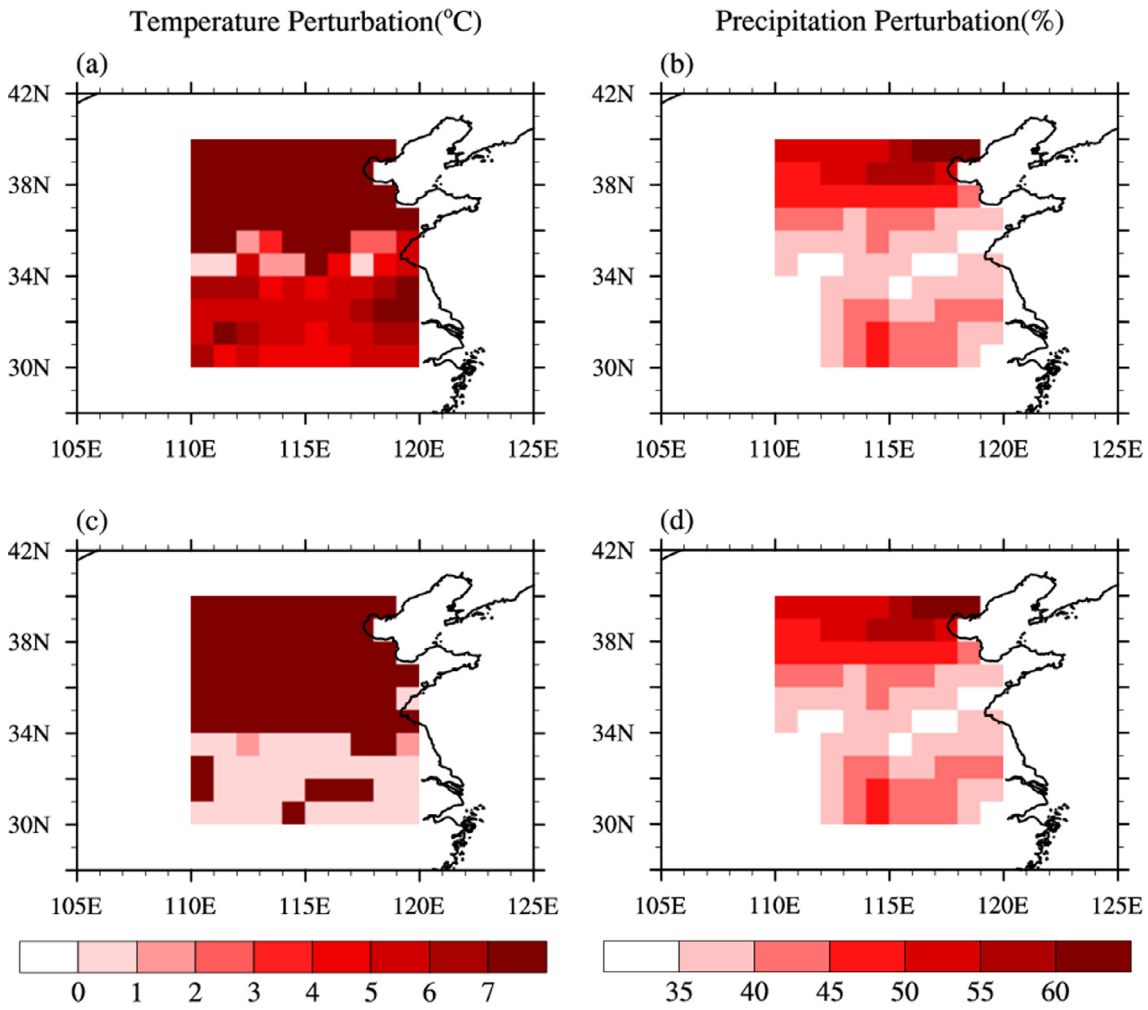

Fig. 2. The perturbations to the annual mean temperature (°C) and total precipitation (%) over the '3H' region in the year 2000 due to the CNOP-P-type scenarios: (a) changes of temperature under the CNOP-P-type temperature change scenario, (b) the percentage changes of precipitation under the CNOP-P-type precipitation change scenario, and (c) changes of temperature and (d) the percentage changes of precipitation under the CNOP-P-type climate change scenarios (including changes in both temperature and precipitation).

Table 3
Descriptions of the climate change scenarios used in this research: Normal, and +5 °C for temperature; Normal and +30% change for precipitation; 'Yes' for the CNOP-P-type scenarios and 'No' for the hypothesized scenarios.

Scenarios	T	P	CNOP-P
The CNOP-P-type temperature change scenario	+5 °C	Normal	Yes
The hypothesized temperature change scenario	+5 °C	Normal	No
The CNOP-P-type precipitation change scenario	Normal	+30%	Yes
The hypothesized precipitation change scenario	Normal	+30%	No
The CNOP-P-type climate change scenario	+5 °C	+30%	Yes
The hypothesized climate change scenario	+5 °C	+30%	No

P.S. 'T' for temperature and 'P' for precipitation. The scenarios obtained by employing the CNOP-P approach are denoted as the CNOP-P-type scenarios, which are indicated by the term 'Yes' in the column 'CNOP-P' of the table. And the term 'No' in the column 'CNOP-P' stands for the hypothesized scenarios, in which a constant (percentage) change is added to the baseline climate condition. Scenarios, in which only changes in temperature (precipitation) are considered, are referred to as the temperature (precipitation) change scenarios. And the scenarios, including the changes in both temperature and precipitation, are referred to as the climate change scenarios.

region was mainly influenced by temperature (Seneviratne et al., 2010) and changed slightly (Fig. 4c1). Consequently, the increased precipitation offset the water loss induced by more Rsur and thus made SSM increase.

3.1.3. Responses of SSM to extreme climate change related to both temperature and precipitation

Here, the maximal responses of SSM to extreme climate change associated with both temperature and precipitation are illustrated by using the CNOP-P approach. For the CNOP-P-type climate change scenario (Figs. 1c and d, Fig. 2c and d), SSM increased in the study region, especially in the north of 35°N (Fig. 5a1). In general, the SSM change varied in the range from +0.008 to +0.047 $m^3\ m^{-3}$ (less than 31.6%).

In the CNOP-P-type climate change scenario, both temperature and precipitation time series are added to positive perturbations. In the north of 35°N, Rsur was altered slightly (Fig. 5d1). Higher Tss occurred (Fig. 5e1), resulting in the melting of soil ice (Fig. 5b1). Soil ice melting along with the increased precipitation jointly led to the SSM increase even though enhanced ET stopped SSM from increasing (Fig. 5c1). In the south, soil ice, ET, and Tss were changed slightly (Fig. 5b1, c1 and e1). More precipitation off-

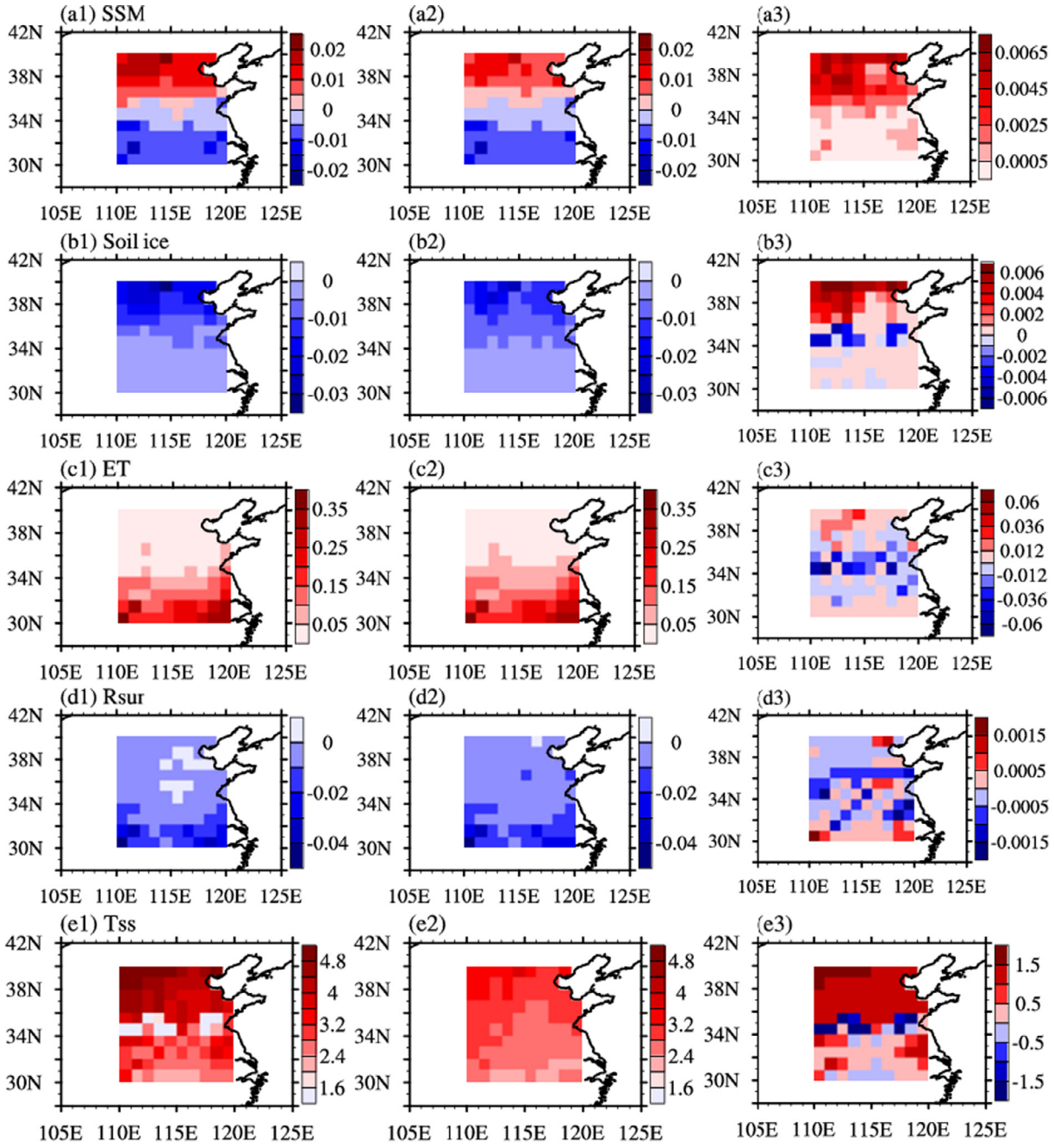

Fig. 3. The spatial variations of SSM, surface soil ice ($m^3\ m^{-3}$), ET, Rsur (mm/day), and Tss (°C) in the year 2000 due to the CNOP-P-type (left panel) and hypothesized (middle panel) temperature change scenarios, and the differences between the variation magnitudes of each variable in the same year under the two scenarios (right panel): the CNOP-P-type scenario minus the hypothesized scenario.

set the water loss caused by the increased Rsur (Fig. 5d1) and contributed to the augment of SSM.

3.2. Comparisons between the responses of SSM to different types of climate change scenarios

In order to make comparisons between the responses of SSM to different types of climate change scenarios, we also analyze the SSM variations under the hypothesized climate scenarios. Three hypothesized scenarios in total (including the hypothesized temperature change scenario, the hypothesized precipitation change scenario, and the hypothesized climate change scenario) are analyzed in this part and have been specifically described in Table 3. As demonstrated above, the difference between the CNOP-P-type scenario and the hypothesized scenario is whether the climate variability is altered or not relative to the reference climate condition. Hence, the importance of climate variability to the responses of SSM to changing climate is explored by analyzing the difference of SSM variations between the two types of climate change scenarios.

Besides, comparisons are only made between the scenarios which take into account the same perturbed climate variable(s). For example, the SSM variations under the CNOP-P-type temperature change scenario are only compared with those under the hypothesized temperature change scenario. In addition, the responses of SSM to the combination of the CNOP-P-type temperature change scenario and the CNOP-P-type precipitation change scenario (referred to as the combined climate change scenario in

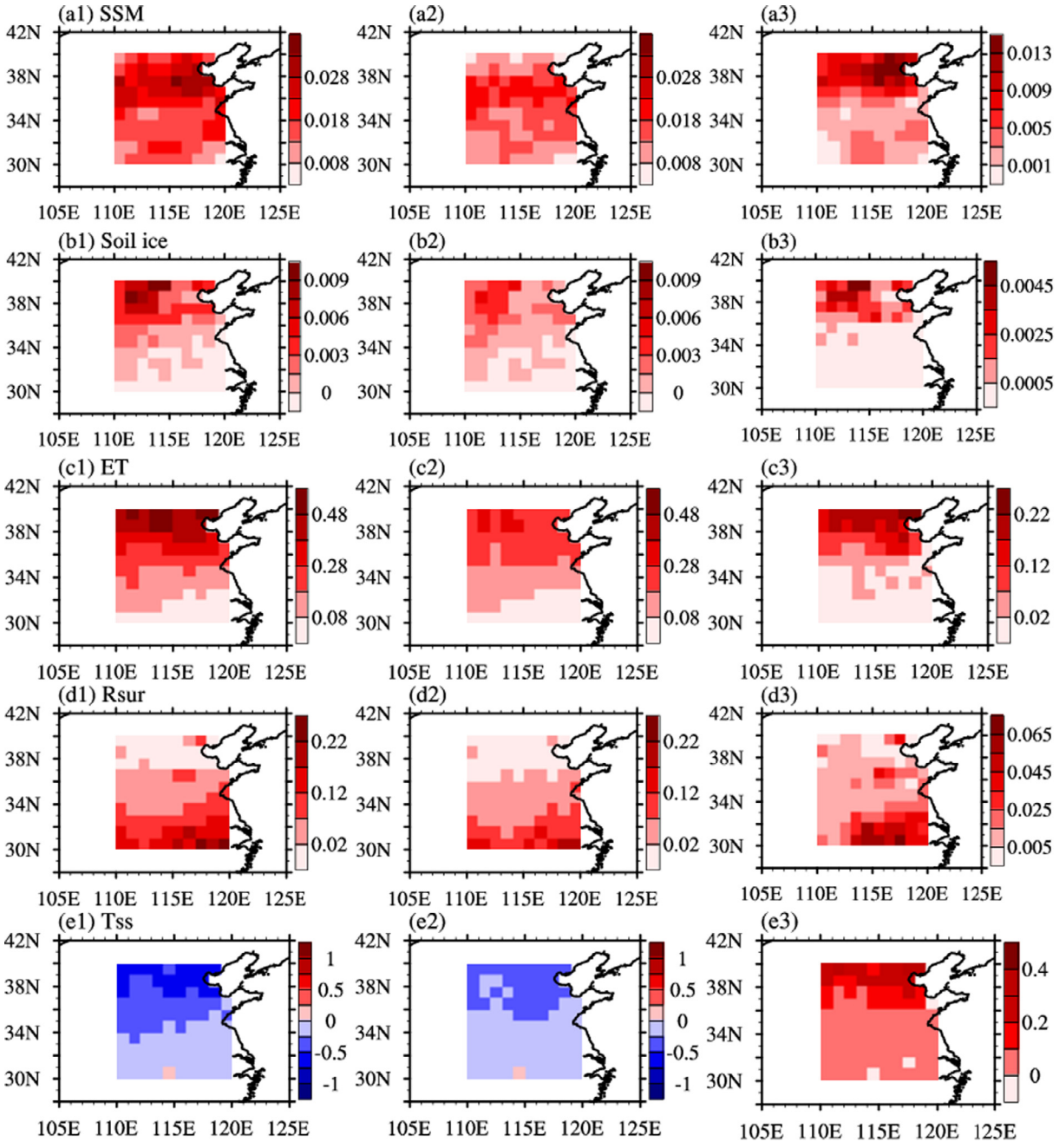

Fig. 4. The spatial variations of SSM, surface soil ice ($m^3\ m^{-3}$), ET, Rsur (mm/day), and Tss (°C) in the year 2000 due to the CNOP-P-type (left panel) and hypothesized (middle panel) precipitation change scenarios, and the differences between the variation magnitudes of each variable in the same year under the two scenarios (right panel): the CNOP-P-type scenario minus the hypothesized scenario.

the following) are also compared with those to the CNOP-P-type climate change scenario.

3.2.1. Comparisons of responses of SSM to different types of only temperature change scenarios

Under the hypothesized temperature change scenario, changes of SSM in the '3H' region (Fig. 3a2) were similar to those under the CNOP-P-type temperature change scenario (Fig. 3a1; In the north: increase; In the south: decrease). But in terms of variation magnitudes, the SSM changes were greater for the latter temperature scenario (Fig. 3a3). And in north of 35°N, the difference between the responses of SSM to the two temperature scenarios was more remarkable than that in the south. The (percentage) changes of regional averaged SSM in the north and south of 35°N further consolidated this (Fig. 6a). In the north, the difference between SSM changes under the two scenarios was 0.003 $m^3\ m^{-3}$ (just 1.9%) while in the south the difference was especially small and could be ignored. It is implied that SSM in the north seems to be more sensitive to temperature variability than that in the south.

To seek for the hydrological processes that could account for the difference between the responses of SSM to different types of scenarios, the variations of hydrological variables (i.e. surface soil ice, ET and Rsur) related to surface water budget as well as Tss were compared between the two temperature change scenarios. In the north of 35°N, changes in ET as well as Rsur under the two scenarios were almost the same (Fig. 3c3 and d3). This had little influence on

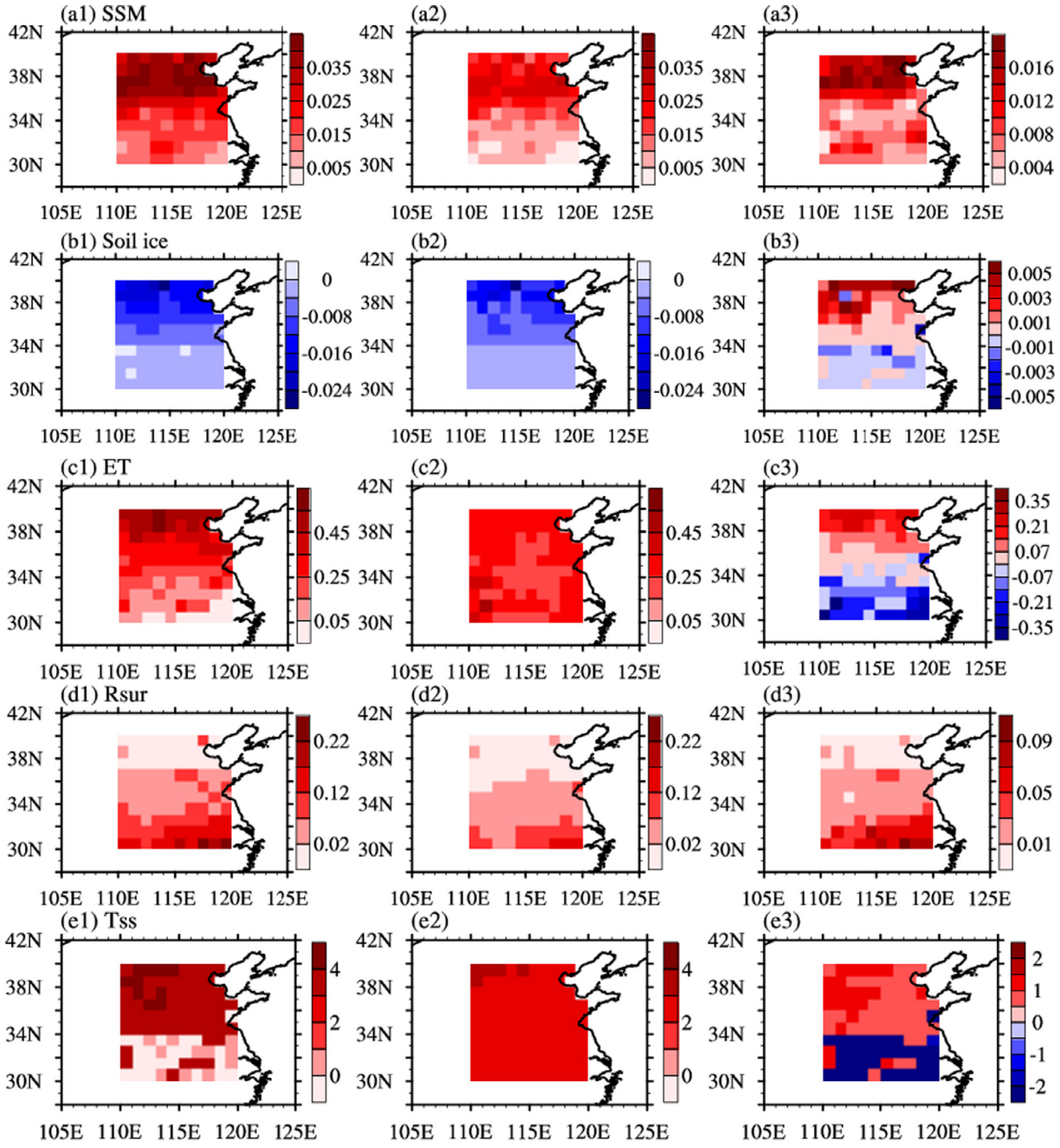

Fig. 5. The spatial variations of SSM, surface soil ice ($m^3\ m^{-3}$), ET, Rsur (mm/day), and Tss (°C) in the year 2000 due to the CNOP-P-type (left panel) and hypothesized (middle panel) climate change scenarios (including changes in both temperature and precipitation), and the differences between the variation magnitudes of each variable in the same year under the two scenarios (right panel): the CNOP-P-type scenario minus the hypothesized scenario.

diversifying the responses of SSM to different scenarios. However, the stronger soil ice melting (Fig. 3b3) induced by the higher Tss (Fig. 3e3) under the CNOP-P-type scenario helped to the greater SSM increase (Fig. 3a3). In the south, changes in soil ice, ET, Rsur and Tss under the two scenarios were almost the same (Fig. 3b3, c3, d3 and e3), resulting in the nearly same SSM responses (Fig. 3a3).

The contributions of seasonal SSM variations to the annual SSM change are also made comparisons between the two types of temperature change scenarios. Since changes on annual time scale are discussed, the season 'winter' mentioned in the following consists of January, February, and December in the same year. As a result, for SSM, the annual change is the average of the variations in all seasons. And the contributions of seasonal SSM variations to the annual SSM change could be represented by the percentages as follows: $100 \times \frac{Seasonal\ SSM\ Changes}{4 \times (Annual\ SSM\ Change)}$. Taking 35°N as a boundary, Fig. 7a describes the contribution of the SSM variation in each season to the annual change in the north and south of the '3H' region, from the view of regional averages. It is exhibited that the main seasonal sources of the annual SSM changes for the two types of scenarios were almost the same. In the north, the signs of SSM changes in all seasons except winter were consistently opposite to that of the annual change. The SSM increase in winter contributed to the annual increase. And in the south, SSM decreased in all seasons, but more dramatically in spring.

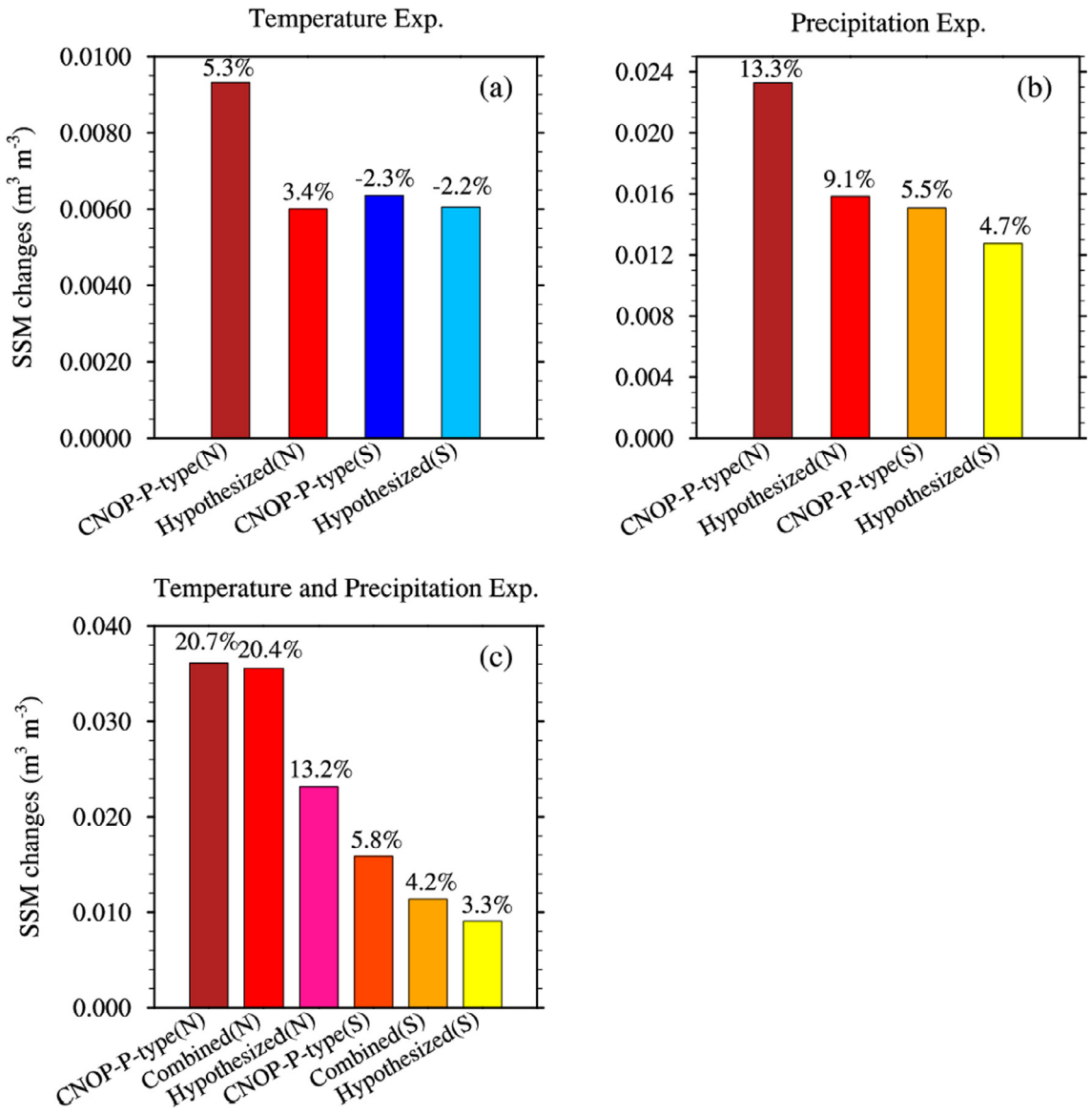

Fig. 6. The changes in regional averaged SSM ($m^3\ m^{-3}$) in the south and north of 35°N of the '3H' region under all climate change scenarios: (a) the CNOP-P-type and hypothesized temperature change scenarios; (b) the CNOP-P-type and hypothesized precipitation change scenarios; (c) the CNOP-P-type, combined and hypothesized climate change scenarios related to both temperature and precipitation (warm colors: increase; cold colors: decrease). The percentage above each bar stands for the percentage change of regional averaged SSM. 'N' represents the northern region and 'S' stands for the southern region.

3.2.2. Comparisons of responses of SSM to different types of only precipitation change scenarios

The responses of SSM to the hypothesized precipitation change scenario are also discussed. Similar to the CNOP-P-type precipitation scenario, the hypothesized scenario led to the increase of SSM (Fig. 4a2). However, the responses of SSM to the CNOP-P-type scenario were greater than those to the hypothesized scenario (Fig. 4a3). And the difference between the responses of SSM to the two scenarios was mainly located in the north of 35°N, where the semi-arid region is located. The (percentage) changes of regional averaged SSM in the north and south of 35°N illustrate this as well (Fig. 6b). In the north, the difference of SSM changes between the two scenarios was 0.007 $m^3\ m^{-3}$ (4.2%) while in the south the difference was only 0.002 $m^3\ m^{-3}$ (0.8%). It is indicated that SSM in the north, where semi-arid region is distributed, is sensitive to precipitation variability.

The variations of hydrological variables (i.e. precipitation, surface soil ice, ET and Rsur) along with Tss are analyzed to explore the reasons for the difference between SSM changes under the two precipitation change scenarios. In the north of 35°N, changes in Rsur under the two scenarios were almost the same (Fig. 4d3). And compared with the hypothesized scenario, the CNOP-P-type scenario caused more soil water freezing (Fig. 4b3) and more ET (Fig. 4c3), which helped to narrow the difference about SSM changes. However, more precipitation widened this difference. In all, different precipitation, soil ice and ET variations under the two scenarios jointly gave rise to the difference between SSM changes. In the south, changes in soil ice, ET, and Tss under the two scenarios were almost the same (Fig. 4b3, c3, and e3). Different precipitation and Rsur changes (Fig. 4d3) mainly contributed to the difference.

As for the contributions of seasonal SSM variations to the annual SSM change, there existed little difference between the two types of precipitation change scenarios (see Fig. 7b). In the north of 35°N, SSM was increased in all seasons and the changes in summer and autumn were the main drivers of the annual

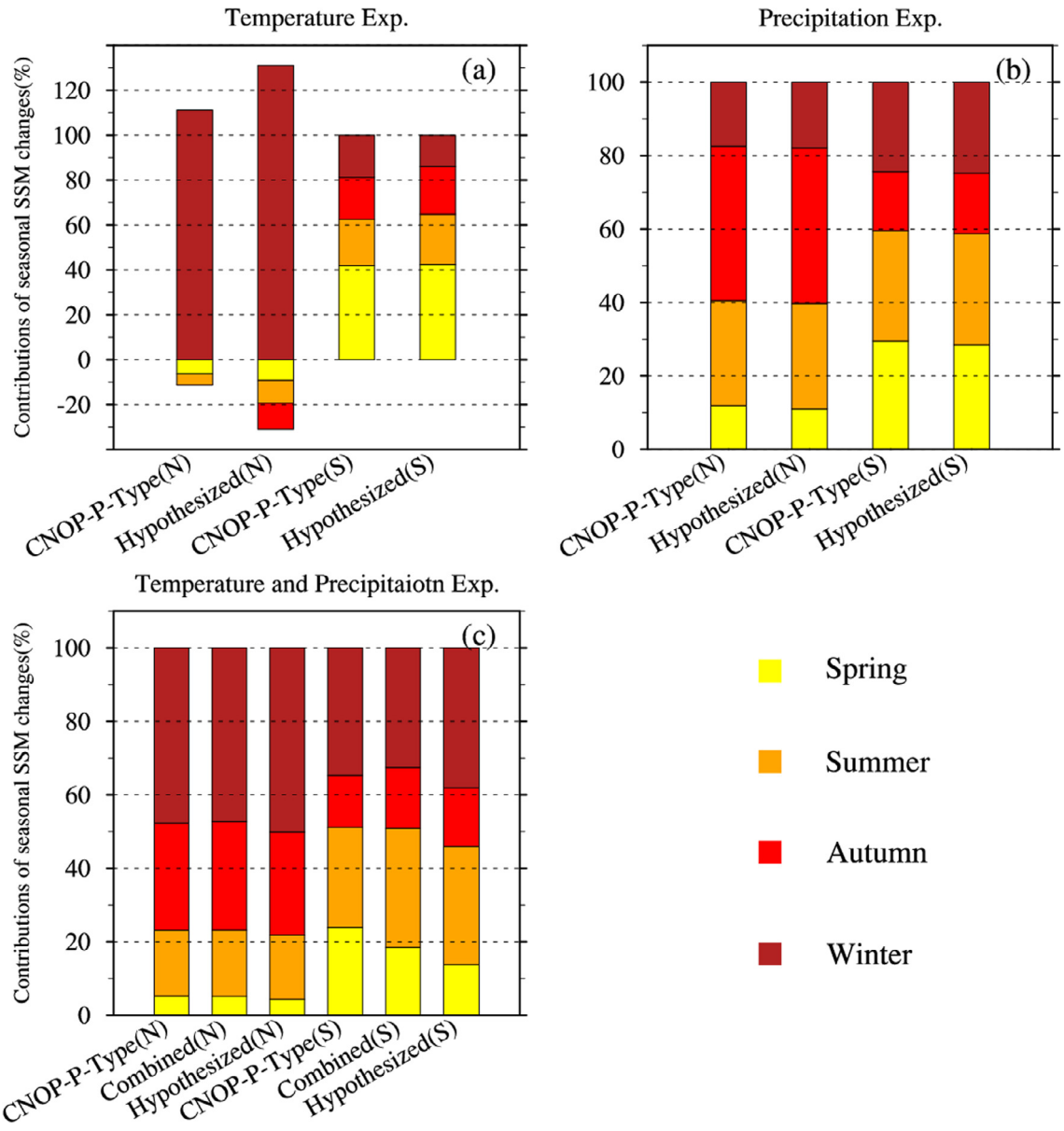

Fig. 7. The contributions of seasonal SSM changes to the annual SSM change (%) in the year 2000 over the north and south of 35°N of the '3H' region under all climate change scenarios: (a) the CNOP-P-type and hypothesized temperature change scenarios; (b) the CNOP-P-type and hypothesized precipitation change scenarios; (c) the CNOP-P-type, combined and hypothesized climate change scenarios related to both temperature and precipitation. 'N' represents the northern region and 'S' stands for the southern region. For the legend, it applies to all of the charts. P.S. As the annual SSM change is the average of the SSM variations in all seasons, the contributions of seasonal SSM variations to the annual SSM change could be measured by the percentages as follows: $100 \times \frac{Seasonal\ \ SSM\ \ Changes}{4 \times (Annual\ \ SSM\ \ Change)}$.

change. In the south, SSM was also augmented in all seasons and the annual SSM change mainly came from variations in spring and summer.

3.2.3. Comparisons between the hypothesized and the CNOP-P-type climate change scenarios

The hypothesized climate change scenario, which reflects changes in both temperature and precipitation, is applied as well. Under this scenario, SSM was increased (Fig. 5a2), similar to that under the CNOP-P-type climate change scenario (Fig. 5a1). However, there existed difference between the SSM variation magnitudes for the two climate change scenarios, which was mainly located in the north of 35°N (Fig. 5a3). The (percentage) changes of regional averaged SSM in the north and south of 35°N demonstrated this similarly (Fig. 6c). In the north, the difference of SSM changes between the two scenarios was 0.013 $m^3\ m^{-3}$ (7.5%) while in the south the difference was 0.007 $m^3\ m^{-3}$ (2.5%). This suggests that the combined effects of both temperature and precipitation variability on SSM are significant, especially in the north of 35°N, where semi-arid region is distributed.

By comparing the variations of hydrological variables and Tss under the two climate change scenarios, the hydrological processes that contribute to the difference between the impacts of different scenarios on SSM are demonstrated. In the north of 35°N, the Rsur variations under the two scenarios were almost the same (Fig. 5d3). More precipitation and more surface soil ice melting due to the higher Tss under the CNOP-P-type scenario (Fig. 5b3 and e3) induced the greater increase of SSM though more ET was bad for this increase (Fig. 5c3). And in the south, the CNOP-P-type scenario led to smaller ET (Fig. 5c3) and lower Tss (Fig. 5e3), both facilitating the retention of soil water. For the changes of soil ice, little difference appeared between the two sce-

narios (Fig. 5b3). Moreover, the greater increase in Rsur for the CNOP-P-type scenario (Fig. 5d3) went against the augment of SSM and helped to lessen the difference between the SSM changes. Generally, different precipitation, ET and Rsur variations under the two scenarios mainly contributed to the difference between SSM changes in the south.

The difference of the contributions of seasonal SSM variations to the annual change between the two types of climate change scenarios is also explored. In the north of 35°N, SSM was increased in all seasons and the SSM changes in autumn and winter were the main sources of the annual SSM change no matter which climate scenario was considered (Fig. 7c). In the south, SSM was also increased in all seasons; nonetheless, the annual SSM change was mainly composed by changes in summer and winter under the hypothesized scenario and in spring, summer and winter under the CNOP-P-type scenario (Fig. 7c). On the whole, the contributions of seasonal SSM variations to the annual SSM change had little to do with the types of climate change scenarios.

3.2.4. Comparisons between the combined climate change scenario and the CNOP-P-type climate change scenarios

In this section, the response of SSM to the combined climate change scenario, which is the combination of the CNOP-P-type temperature scenario and the CNOP-P-type precipitation change scenario, is reported. Similar to the CNOP-P-type climate change scenario, it induces the changes in both temperature and precipitation variability. Due to this combined scenario, SSM increased in the '3H' region. And compared with the CNOP-P-type scenario, the combined scenario caused similar responses of SSM in the north of 35°N but smaller responses in the remaining region. Take 35°N as a boundary. Fig. 7c describes the regional averaged SSM variations in the north and south. For the northern region, the changes of SSM for the two scenarios were almost the same. Within the southern region, the difference of SSM variations between the two scenarios was 0.005 $m^3\ m^{-3}$ (1.6%). And the greater SSM responses to the CNOP-P-type climate change scenario were mainly attributed to the smaller increase of ET. As for the contributions of seasonal SSM changes to the annual change, little difference existed between the two types of scenarios (see Fig. 7c).

In summary, the spatial distribution of SSM changes under the CNOP-P-type scenario associated with temperature or precipitation was similar to that under the corresponding hypothesized scenario related to temperature or precipitation. However, there still existed difference between the responses of SSM to the two types of scenarios. In terms of variation magnitude, the changes of SSM under the CNOP-P-type scenario were greater than those under its corresponding hypothesized scenario, especially in the north of 35°N. The difference between the responses of SSM to the two types of scenarios reveals that climate variability plays an important role in the SSM changes in the north of 35°N of the '3H' region, where semi-arid region is located. In this northern region, different SSM changes between the two types of temperature scenarios were mainly attributed to different soil ice changes. Between the two precipitation change scenarios, the difference of precipitation changes primarily contributed to the difference of SSM changes, although the differences of both soil ice and ET changes had the impacts of narrowing this difference associated with SSM. For the two climate change scenarios (i.e. the CNOP-P-type climate change

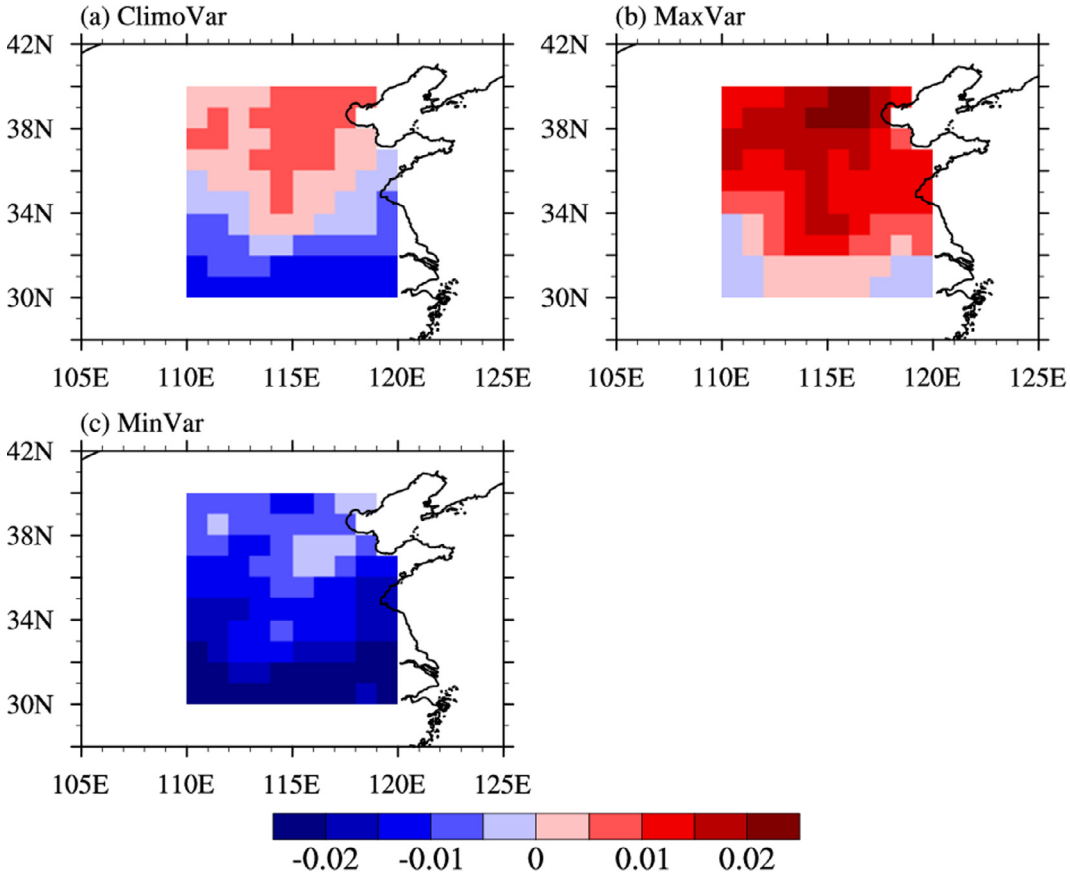

Fig. 8. The simulated annual SSM changes ($m^3\ m^{-3}$) from 7 CMIP5 GCMs with higher spatial resolutions, all of which are bilinear-interpolated to the resolution of 1° × 1°, under the RCP8.5 scenario during the end of 21st century (2071–2100) relative to the period 1961–1990: (a) changes in climatology; (b) maximal changes; (c) minimal changes.

scenario and the hypothesized climate change scenario), the differences in both precipitation and soil ice changes resulted in the difference about SSM changes even though the difference about ET variations helped to lessen the difference about SSM.

Besides, the comparisons between the responses of SSM to the CNOP-P-type climate change scenario and the combined climate change scenario (i.e. the combination of the CNOP-P-type temperature scenario and the CNOP-P-type precipitation change scenario) are also made. But the difference of SSM changes between the two climate scenarios was mainly located in the south of 35°N of the study region, which was mainly caused by different ET variations.

4. Discussions

As a reference, the future possible SSM changes based on multi-model ensemble averages are evaluated in the '3H' region by using simulations from 7 CMIP5 GCMs with higher spatial resolutions (in bold font in Table 2). As there exists difference between the spatial resolutions of the 7 GCMs, the model data are all bilinear-interpolated to the resolution of $1° \times 1°$. Fig. 8 presents the annual mean, maximal and minimal SSM changes under the RCP8.5 scenario during the end of the 21st century (2071–2100) relative to the period 1961–1990. It is exhibited that the climatology of SSM is increased in the north of about 35°N and reduced in the south, but the climatological changes generally don't exceed 0.01 $m^3\ m^{-3}$. And the annual SSM changes, which could be bounded by the minimal and maximal SSM changes (Fig. 8b and c), usually vary in the range from −0.02 to +0.02 $m^3\ m^{-3}$. The changes in SSM (from +0.008 to +0.047 $m^3\ m^{-3}$) under the CNOP-P-type climate change scenario, which includes the changes in both temperature and precipitation, are greater than above-mentioned SSM changes derived from GCMs. To some extent, the two kinds of SSM variations are consistent. As the SSM changes induced by the CNOP-P-type climate change scenario suggest the maximal possible SSM variations within a kind of certain reasonable range of future climate change by the end of the 21st century.

Dan et al. (2012) evaluated the hydrological changes under the hypothesized precipitation and temperature changes with the VIC model in the 3H region of China (113°E–the coastline, 32°–40.5°N), which is smaller than our study region (110°E ∼ 120°E, 30°–40°N). For the hypothesized scenarios with a 5 °C warming or a 30% increase in precipitation, only SSM changes averaged over the whole 3H region were exhibited in their study. When only temperature was changed, SSM was decreased slightly. When changes in both temperature and precipitation were considered, SSM increased by about 2%. However, under the CNOP-P-type temperature scenario, SSM averaged in the '3H' region was slightly increased. For the CNOP-P-type scenarios related to both temperature and precipitation, regional averaged SSM increased by about 11%. These differences may be induced by the different hydrological models, climate scenarios, study periods and forcing datasets.

5. Conclusions

Based on the future potential climate change by the end of the 21st century under a higher future greenhouse gas emission (RCP8.5), the maximal responses of SSM to an extreme condition of climate change in the '3H' region (110°–120°E, 30°–40°N) is discussed by using the CoLM model and CNOP-P approach in this study. To explore the responses of SSM to different types of climate scenarios, the hypothesized climate change scenarios are also employed. What's more, comparisons are conducted between the scenarios which consider the same perturbed climate variable(s). Consequently, the importance of climate variability to SSM could be analyzed through comparing the responses of SSM to the two different types of scenarios.

Results have demonstrated that the two types of climate change scenarios associated with extreme change in temperature or precipitation induced similar SSM changes. In response to climate scenarios only related to temperature change, SSM was increased in the north of 36°N of the '3H' region and was reduced in the south. For only precipitation change scenarios, SSM was increased in the whole study region. Similar to the precipitation change scenarios, the scenarios associated with both temperature and precipitation changes also induced the augment of SSM in the whole '3H' region. However, there existed difference between the responses of SSM to the two types of scenarios in terms of variation magnitude. The possible maximal variations of soil moisture could be supplied with considering the variations of the climate variability based on the character of the CNOP-P approach. And the difference between the absolute changes of SSM under the two types of climate scenarios was mainly located in the north of 35°N, where the semi-arid region is located. This implies that the climate variability plays the important role in estimating the variation of soil moisture in the semi-arid region of China.

Taking 35°N as a boundary, the '3H' region is divided into two sub-regions. And the difference of changes in regional averaged SSM between different types of temperature (or precipitation) scenarios is displayed for each sub-region. Between the two types of climate change scenarios, in which both temperature and precipitation are changed, the difference of SSM changes within the north of 35°N was most remarkable (7.5%). This further underlines the important role of climate variability in the SSM changes over the semi-arid region, which is consistent with the study of Koster et al. (2004). Besides, the contributions of seasonal SSM changes to the annual change are also analyzed and found to be nearly independent on the types of climate change scenarios, from the standpoint of regional averages. Details are not repeated here.

Moreover, as there are deficiencies in model's structure and parameters, model parameter calibrations and validations, and other hydrological models should be included in future work. For this study, climate change is only represented by variations of temperature and precipitation. In fact, it also includes changes in other climatic variables, e.g. solar irradiance and atmospheric CO_2 concentration. Robock and Li (2006) have addressed the vital impacts of solar radiation and CO_2 on soil moisture trends. It is therefore necessary to pay attention to the changes in multiple climatic variables (not just temperature and precipitation) in future researches about the responses of soil moisture to the changing climate.

Acknowledgment

Funding was provided by Grants from the National Natural Science Foundation of China (Nos. 91437111, 41675104, 41375111, 40830955).

References

Chen, H., 2013. Projected change in extreme rainfall events in China by the end of the 21st century using CMIP5 models. Chin. Sci. Bull. 58, 1462–1472.
Chen, H., Sun, J., Chen, X., Zhou, W., 2012. CGCM projections of heavy rainfall events in China. Int. J. Climatol. 32, 441–450.
Dai, Y.J. et al., 2003. The common land model. Bull. Am. Meteorol. Soc. 84, 1013–1023.
Dan, L., Ji, J., Xie, Z., Chen, F., Wen, G., Richey, J.E., 2012. Hydrological projections of climate change scenarios over the 3H region of China: a VIC model assessment. J. Geophys. Res. 117, D11102. http://dx.doi.org/10.1029/2011JD017131.
Duan, Q., Sorooshian, S., Gupta, V., 1992. Effective and efficient global optimization for conceptual rainfall-runoff models. Water Resour. Res. 28, 1015–1031.
Duan, W.S., Mu, M., 2006. Investigating decadal variability of El Nino-Southern Oscillation asymmetry by conditional nonlinear optimal perturbation. J. Geophys. Res. 111, C07015. http://dx.doi.org/10.1029/2005JC003458.

Duan, W.S., Zhang, R., 2010. Is model parameter error related to a significant spring predictability barrier for El Niño events? Results from a theoretical model. Adv. Atmos. Sci. 27, 1003–1013.
Duan, W.S., Mu, M., Wang, B., 2004. Conditional nonlinear optimal perturbations as the optimal precursors for El Nino-Southern Oscillation events. J. Geophys. Res. 109, D23105. http://dx.doi.org/10.1029/2004JD004756.
Heim, R.R., 2002. A review of twentieth-century drought indices used in the United States. Bull. Am. Meteorol. Soc. 83, 1149–1165.
Ji, D., Wang, L., Feng, J., Wu, Q., Cheng, H., Zhang, Q., Yang, J., Dong, W., Dai, Y., Gong, D., Zhang, R.-H., Wang, X., Liu, J., Moore, J.C., Chen, D., Zhou, M., 2014. Description and basic evaluation of Beijing Normal University Earth System Model (BNU-ESM) version 1. Geosci. Model Dev. 7, 2039–2064. http://dx.doi.org/10.5194/gmd-7-2039-2014.
Jiang, Z., Song, J., Li, L., Chen, W., Wang, Z., Wang, J., 2012. Extreme climate events in China: IPCC-AR4 model evaluation and projection. Clim. Change 110, 385–401.
Kanae, S., Hirabayashi, Y., Yamada, T., Oki, T., 2006. Influence of "realistic" land surface wetness on predictability of seasonal precipitation in boreal summer. J. Clim. 19, 1450–1460.
Kim, Y., Wang, G., 2012. Soil moisture-vegetation-precipitation feedback over North America: its sensitivity to soil moisture climatology. J. Geophys. Res. Atmos. 117, D18115. http://dx.doi.org/10.1029/2012JD017584.
Koster, R.D. et al., 2010. Contribution of land surface initialization to subseasonal forecast skill: first results from a multi-model experiment. Geophys. Res. Lett. 37, L02402. http://dx.doi.org/10.1029/2009GL041677.
Koster, R.D. et al., 2004. Regions of strong coupling between soil moisture and precipitation. Science 305, 1138–1140.
Li, M., Ma, Z., 2010. Comparisons of simulations of soil moisture variations in the Yellow River basin driven by various atmospheric forcing data sets. Adv. Atmos. Sci. 27, 1289–1302.
Liu, D., Wang, G., Mei, R., Yu, Z., Yu, M., 2014. Impact of initial soil moisture anomalies on climate mean and extremes over Asia. J. Geophys. Res. Atmos. 119, 529–545.
Liu, S., Lin, Z., 2005. Validation of common land model using field experiment data over typical land cover types in East Asia. Clim. Environ. Res. 10, 684–699 (in Chinese).
Ma, Z.G., Fu, C.B., 2005. Decadal variations of arid and semi-arid boundary in China. Chin. J. Geophys. 48, 519–525 (in Chinese).
Mehrotra, R., 1999. Sensitivity of runoff, soil moisture and reservoir design to climate change in central Indian River basins. Clim. Change 42, 725–757.
Mostovoy, G.V., Anantharaj, V.G., 2008. Observed and simulated soil moisture variability over the lower Mississippi delta region. J. Hydrometeor. 9, 1125–1150.
Mu, M., Wang, B., 2007. Nonlinear instability and sensitivity of a theoretical grassland ecosystem to finite-amplitude perturbations. Nonlinear Processes Geophys. 14, 409–423.
Mu, M., Jiang, Z., 2008. A new approach to the generation of initial perturbations for ensemble prediction: conditional nonlinear optimal perturbation. Chin. Sci. Bull. 53, 2062–2068 (in Chinese).
Mu, M., Duan, W.S., Wang, B., 2003. Conditional nonlinear optimal perturbation and its applications. Nonlinear Processes Geophys. 10, 493–501.
Mu, M., Sun, L., Dijkstra, H.A., 2004. The sensitivity and stability of the ocean's thermohaline circulation to finite-amplitude perturbations. J. Phys. Oceanogr. 34, 2305–2315.
Mu, M., Zhou, F., Wang, H., 2009. A method for identifying the sensitive areas in targeted observations for tropical cyclone prediction: conditional nonlinear optimal perturbation. Mon. Weather Rev. 137, 1623–1639.
Mu, M., Duan, W.S., Wang, Q., Zhang, R., 2010. An extension of conditional nonlinear optimal perturbation approach and its applications. Nonlinear Processes Geophys. 17, 211–220.
Qin, X., Duan, W.S., Mu, M., 2013. Conditions under which CNOP sensitivity is valid for tropical cyclone adaptive observations. Q. J. R. Meteorol. Soc. 139, 1544–1554.
Robock, A., Li, H., 2006. Solar dimming and CO_2 effects on soil moisture trends. Geophys. Res. Lett. 33, L20708. http://dx.doi.org/10.1029/2006GL027585.
Seager, R., Ting, M., Li, C., Naik, N., Cook, B., Nakamura, J., Liu, H., 2013. Projections of declining surface-water availability for the southwestern United States. Nat. Clim. Change 3, 482–486.
Seneviratne, S.I. et al., 2010. Investigating soil moisture–climate interactions in a changing climate: a review. Earth Sci. Rev. 99, 125–161.
Sheffield, J., Goteti, G., Wood, E.F., 2006. Development of a 50-year high-resolution global dataset of meteorological forcings for land surface modeling. J. Clim. 19, 3088–3111.
Singh, P., Bengtsson, L., 2004. Hydrological sensitivity of a large Himalayan basin to climate change. Hydrol. Process. 18, 2363–2385.
Song, Y., Guo, W., Zhang, Y., Chen, Y., 2009. Performances of CoLM and NCAR_CLM3.0 in simulating land-atmosphere interactions over typical forest ecosystems in China Part I. Preliminary analysis of the simulations based on different models. Clim. Environ. Res. 14, 229–242 (in Chinese).
Storn, R., Price, K., 1997. Differential evolution – a simple and efficient heuristic for global optimization over continuous spaces. J. Global Optim. 11, 341–359.
Sun, G.D., Mu, M., 2011. Nonlinearly combined impacts of initial perturbation from human activities and parameter perturbation from climate change on the grassland ecosystem. Nonlinear Processes Geophys. 18, 883–893.
Sun, G.D., Mu, M., 2012. Responses of soil carbon variation to climate variability in China using the LPJ model. Theor. Appl. Climatol. 110, 143–153.
Sun, G.D., Mu, M., 2013. Understanding variations and seasonal characteristics of net primary production under two types of climate change scenarios in China using the LPJ model. Clim. Change 120, 755–769.
Sun, G.D., Mu, M., 2014. The analyses of the net primary production due to regional and seasonal temperature differences in eastern China using the LPJ model. Ecol. Model. 289, 66–76.
Tao, F., Yokozawa, M., Hayashi, Y., Lin, E., 2003. Future climate change, the agricultural water cycle, and agricultural production in China. Agric. Ecosyst. Environ. 95, 203–215.
Taylor, K.E., Stouffer, R.J., Meehl, G.A., 2012. An overview of CMIP5 and the experiment design. Bull. Am. Meteorol. Soc. 93, 485–498.
Wang, A., Lettenmaier, D.P., Sheffield, J., 2011. Soil moisture drought in China, 1950–2006. J. Clim. 24, 3257–3271.
Wang, B., Huo, Z., 2013. Extended application of the conditional nonlinear optimal parameter perturbation method in the common land model. Adv. Atmos. Sci. 30, 1213–1223.
Wang, L., Chen, W., 2014. A CMIP5 multimodel projection of future temperature, precipitation, and climatological drought in China. Int. J. Climatol. 34, 2059–2078.
Wang, Q., Mu, M., Dijkstra, H., 2012. Application of the conditional nonlinear optimal perturbation method to the predictability study of the Kuroshio large meander. Adv. Atmos. Sci. 29, 118–134.
Wang, Q., Mu, M., Dijkstra, H.A., 2013. Effects of nonlinear physical processes on optimal error growth in predictability experiments of the Kuroshio Large Meander. J. Geophys. Res. Oceans 118, 6425–6436.
Wilson, D.J., Western, A.W., Grayson, R.B., 2004. Identifying and quantifying sources of variability in temporal and spatial soil moisture observations. Water Resour. Res. 40, W02507. http://dx.doi.org/10.1029/2003WR002306.
Xin, Y., Bian, L., Zhang, X., 2006. The application of CoLM to arid region of northwest China and Qinghai-Xizang Plateau. Plateau Meteorol. 25, 567–574 (in Chinese).
Xu, J., Shu, H., 2014. Assimilating MODIS-based albedo and snow cover fraction into the Common Land Model to improve snow depth simulation with direct insertion and deterministic ensemble Kalman filter methods. J. Geophys. Res. Atmos. 119, 10684–10701. http://dx.doi.org/10.1002/2014JD022012.
Yang, K., Ye, B., Zhou, D., Wu, B., Foken, T., Qin, J., Zhou, Z., 2011. Response of hydrological cycle to recent climate changes in the Tibetan Plateau. Clim. Change 109, 517–534.
Yapo, P.O., Gupta, H.V., Sorooshian, S., 1998. Multi-objective global optimization for hydrologic models. J. Hydrol. 204, 83–97.
Yu, Y., Mu, M., Duan, W.S., 2011. Does model parameter error cause a significant "spring predictability barrier" for El Niño events in the Zebiak-Cane model? J. Clim. 25, 1263–1277.
Zhang, R., Zuo, Z., 2011. Impact of spring soil moisture on surface energy balance and summer monsoon circulation over East Asia and precipitation in East China. J. Clim. 24, 3309–3322.
Zhang, Y., Xu, Y., Dong, W., Cao, L., Sparrow, M., 2006. A future climate scenario of regional changes in extreme climate events over China using the PRECIS climate model. Geophys. Res. Lett. 33, L24702. http://dx.doi.org/10.1029/2006GL027229.
Zuo, Z., Zhang, R., 2007. The spring soil moisture and the summer rainfall in eastern China. Chin. Sci. Bull. 52, 3310–3312.